NUMERICAL STUDY OF THE COMBUSTION OF CONVENTIONAL AND BIOFUELS USING REDUCED AND ADVANCED REACTION MECHANISMS

by

Ibrahim E. ABDALLA [a*], Ayedh ALAJMI [a], and Zhiyin YANG [b]

[a] Faculty of Technology, De Montfort University, Leicester, UK
[b] Department of Engineering and Design, University of Sussex, Brighton, UK

Original scientific paper
DOI: 10.2298/TSCI141106038A

Combustion process of conventional liquid fuels and biofuels depend on many factors including thermo-physicochemical properties associated with such fuels, their chemical structure and the combustion infrastructure used. This manuscript summarises the computational results of a steady CFD simulation for reactive flows performed to validate advanced reaction mechanisms for both conventional and biofuels. The computational results have shown good agreement with the available experimental data with the differences thoroughly discussed and explained. An important observations and findings reported in this work was that when comprehensive reaction models were used, the injected fuels burned at a slower rate compared to the situation when reduced models were employed. While such comprehensive models predicted better flame structure and far better biproducts compared to the existing experimental results, it has also led to over-predicting the temperature field. The computational results have also shown that biodiesel produces a marginally higher rate of carbon dioxide compared to diesel. Such results are thought to be due to the oxygenated nature of the fuel and how such feature influences the development of a comprehensive reaction mechanism for such fuels.

Key words: *combustion, conventional and biofuels, reaction mechanisms, emissions*

Introduction

Liquid fuels extracted from crude petroleum or produced from renewable sources are predicted to remain the main sources of energy for long time to come. Liquid fuels produced from vegetables (or animal fat sources) are considered as renewable taking into consideration the fact that the plants from which they are produced absorb most if not all of CO_2 such fuels produce as a result of burning them. For more reviews on this topic the reader is advised to consult with a recently published review paper by Nigama and Singh [1] and other relevant publications including the work of Demirbas [2] as a few examples.

For an optimal use of biofuels by the existing combustion infrastructure (combustion chambers in internal combustion engines or other burners), an effective combustion process is essential to ensure the maximum energy is extracted from biofuels while reducing the emission

* Corresponding author; e-mail: iabdalla@dmu.ac.uk

rates of harmful pollutant carbon oxides (CO_x) and nitrogen oxides (NO_x) among others. The rate of emission of such gases is a function of many parameters, some of them can be described as macro-scale parameters (such as the equivalence ratio, Φ) while others are associated with a much smaller (micro-scale) features of the combustion process such as the chemical reactions and how such reaction proceed under different temperatures and pressures. The two types of parameters are not independent and they impact each other in a quite complex fashion. While it is easy to change and understand the effects of changing such macroscopic parameters on the combustion process, the microscopic parameters such as the reaction mechanism necessary to model the burning of liquid or gaseous hydrocarbons under a specific environment have been and still poses a challenge.

There is some evidence that biofuels produce less emission of such harmful gases compared to conventional fuels when burned under specific controlled environment although this fact/statement is debatable [3]. The in-depth reason why biofuels produce less emission compared to conventional ones is not fully explained so far. A typical example of conventional hydrocarbon is n-decane ($C_{10}H_{22}$), the closest biofuels to it is methyl decanoate ($C_{11}H_{22}O_2$). It is apparent that the fundamental difference between the two hydrocarbons is the existence of two oxygen atoms in biodiesel which changes the bonding of hydrogen to carbon atoms in the later. Therefore, one would expect that the way these hydrocarbons react and burn in a stream of air will differ.

There are some broad-meaning statements in the literature that attribute the decrease in emission from biofuels combustion compared to conventional ones to the existence of an oxygen atoms in the chemical structure of biofuels. Presumably this is the reason, one would conclude that it is down to the way this oxygen atom influence the reactions paths and rates. Hence, the reaction mechanism that is used in modelling reactive flows is crucial and needs careful consideration. A comprehensive reaction mechanism is not only necessary to predict the heat liberated from the combustion but also the byproducts of the combustion and hence a complete picture of the combustion process.

Based on these arguments and the discussion presented in the previous paragraphs, the main goal of this paper is to present computational results for the spray combustion of different hydrocarbon (both conventional and biofuels) using reduced and advanced reaction mechanisms. The objectives behind the study can be summarised in two parts. The first is to develop, study the difference, test and validate a specific reaction mechanism for the combustion of methanol used in the experimental studies of Widman and Presser [4] and hence develop more mechanisms to model the combustion of other hydrocarbons that represent conventional and biofuels. The second objective is to perform comprehensive analysis for the computational results and comment on the amount of energy liberated and emission produced from the combustion of conventional and biofuels from the CFD predictions based on such advanced reaction mechanisms.

It is worth to mention the fact that the exact work of Widman and Presser [4] has been modelled only once by Collazo *et al.* [5] who used basic combustion model in the form of eddy dissipation concept model. This study adopted the steady laminar flamelet model (SLFM) for modelling the reactive flow under consideration.

Computational domain and the method used

The computations performed in this manuscript are based on steady CFD techniques using Reynolds-averaged Navier-Stokes equation (RANS). Detail mathematical formulation for the equation describing reactive flows can be found in Poinsot and Veynante [6] and in many textbooks too. The equations governing flows with chemical reactions are the continuity, the

momentum, the species conservation equations and the energy. The Favre averaged governing equations can be written:

– *conservation of mass*

$$\frac{\partial \overline{\rho}}{\partial t} + \frac{\partial}{\partial x_i}(\overline{\rho}\widetilde{u}_i) = 0 \tag{1}$$

– *conservation of momentum*

$$\frac{\partial \overline{\rho}\widetilde{u}_i}{\partial t} + \frac{\partial}{\partial x_i}(\overline{\rho}\widetilde{u}_i\widetilde{u}_j) + \frac{\partial \overline{p}}{\partial x_j} = \frac{\partial}{\partial x_i}(\overline{\tau}_{i,j} - \overline{\rho}\,\widetilde{u_i''u_j''}) \tag{2}$$

where the viscous stress tensor $\tau_{i,j}$ for a Newtonian fluid and incompressible flow is given:

$$\tau_{i,j} = 2\frac{\mu}{\rho}S_{ij} \tag{3}$$

where μ is the laminar dynamic viscosity, and S_{ij} – the strain rate tensor defined:

$$S_{ij} = \frac{1}{2}\left(\frac{\partial \widetilde{u}_i}{\partial x_j} + \frac{\partial \widetilde{u}_j}{\partial x_i}\right) \tag{4}$$

– *conservation of chemical species*

$$\frac{\partial(\overline{\rho}\widetilde{Y}_k)}{\partial t} + \frac{\partial}{\partial x_i}(\overline{\rho}\widetilde{u}_i\widetilde{Y}_k) = -\frac{\partial}{\partial x_i}(\overline{V_{k,i}Y_k} + \overline{\rho}\,\widetilde{u_i''Y_k''}) + \overline{\dot{\omega}}_k \tag{5}$$

where $k = 1, 2,..., N$ species,

– *conservation of energy*

$$\frac{\partial \overline{\rho}\widetilde{h}_s}{\partial t} + \frac{\partial}{\partial x_i}(\overline{\rho}\widetilde{u}_i\widetilde{h}_s) = \overline{\dot{\omega}}_T + \frac{\overline{Dp}}{Dt} + \frac{\partial}{\partial x_i}\left(\overline{\lambda\frac{\partial T}{\partial x_i}} - \overline{\rho u_i''h_s''}\right) + \overline{\tau_{i,j}\frac{\partial u_i}{\partial x_j}} - \frac{\partial}{\partial x_i}\left(\overline{\rho\sum_{k=1}^{N}h_{s,k}Y_kV_{k,i}}\right) \tag{6}$$

where

$$\frac{\overline{DP}}{Dt} = \frac{\partial \overline{p}}{\partial t} + \overline{u_i\frac{\partial p}{\partial x_i}} = \frac{\partial \overline{p}}{\partial t} + \widetilde{u}_i\frac{\partial \overline{p}}{\partial t} + \overline{u''\frac{\partial p}{\partial x_i}} \tag{7}$$

– *any conserved scalar (such as mixture fraction)*:

$$\frac{\partial}{\partial t}(\overline{\rho}\widetilde{Z}) + \frac{\partial}{\partial x_i}(\overline{\rho}\widetilde{u}_k\widetilde{Z}) = \frac{\partial}{\partial x_i}(\widetilde{D}^z) - \frac{\partial}{\partial x_i}(\rho\,\widetilde{u_k''Z''}) \tag{8}$$

This averaging procedure introduces unclosed quantities that have to be modelled. The shear-stress transport (SST) *k-ω* [7] turbulence model was employed to close the RANS equation. The SLFM, based on mixture fraction concept [8] was used to model the combustion process. Air-blast/air-assist atomizer model was used in atomising the liquid fuel. The radiation model used in the present study is the P-1 model. For more details on this the reader may refer to the implementation of these models in Fluent Ansys 12.1 [9], the code used to perform the computations. The CHMKIN-CFD and EXGAS [10] were used to facilitate the generation and the use of an advanced reaction models as will be presented later.

Reaction mechanism development

Developing a reaction mechanism based on specific parameters has been made possible through few studies in-cluding the work of Ranzi *et al.* [11] and others. In this work, an aid software EXGAS (fig. 1) was used to generate the necessary reaction mechanism. Most of the

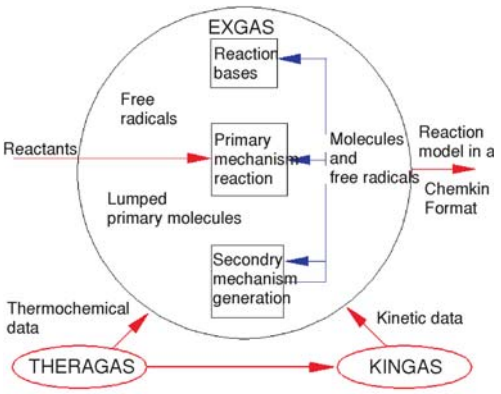

Figure 1. General description of the EXGAS system

necessary types of reaction were involved. These include base, primary and secondary reactions which in terms includes reactions associated with alkanes, alkenes, alcohol, ketone, aldehyde, Diels Adler, and terminations reactions. Formations of Allylic free radicals (by metathesis) as well as reactions of allylic free radicals on alkenes were used as representatives for radicals. The reader is advised to refer to a couple of publications including the work of Herbinet *et al*. [12] and others for detailed information on how such reactions are coupled. The software generates reaction mechanisms compatible with CHEMKIN-CFD for Ansys Fluent and hence the use of the flamelet model. Other data were taken from relevant web sites, specifically the thermal data from Burcast [13].

Table 1. Chemical reaction mechanisms

Fuel/Mechanism	Number of reactions	Number of species
Methanol/SDRM	50	322
Methanol/EGRM	62	799
n-decane/EGRM	160	1726

In addition to the developed "EXGAS reaction mechanisms" (EGRM), the well-known *San Diego Mechanism* SDRM [14] was also used. The model was mainly relevant to modelling flames, high temperature combustion for light hydrocarbons. In comparison to the developed reaction mechanism in this study, the SDRM is considered as reduced one as the number of species and reactions are kept to the minimum needed to describe the systems and phenomena addressed, thereby minimizing as much as possible the uncertainties in the rate parameters employed (tab. 1). In one way this is good as the results obtained using this mechanism have less uncertainties, however, if completeness of the combustion process is sought, the model may fall short of achieving this goal – which is the point the authors of this manuscript are aware.

Benchmark and computational domain

The experimental database and benchmark adopted for validation of the reaction mechanisms used to model the spray combustion of conventional and biofuels was that of Widman and Presser [4]. The 3-D CFD model for the burner used in this study and the mesh is shown in fig. 2. The inner view shows both the injector position as well as the air inflow boundary. The mesh was made quite fine in regions where high gradients of turbulence and/or temperature gradients are expected in order to resolve the physics of fluid in these regions. Some initial trails have been conducted with different meshes of order 750,000 and 1.5 million mesh cell, however, the mesh shown in fig. 2 consist of more than two millions finite element and it is the mesh adopted in the current simulation.

In Widmann and Presser [4] experiment, liquid methanol (CH_3OH) was sprayed and burned within the burner geometry described above under specific operating boundary condition detailed in tab. 2. They obtained a range of data including temperature, velocity fields and emission for carbon oxides, (CO, CO_2), using thermo-couples and some gas analysers at the exit region of the computational domain. In the current CFD model for the base case of Widmann

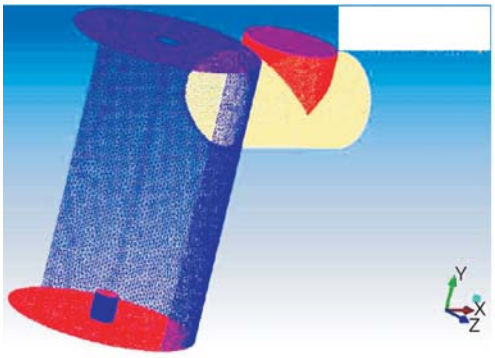

Figure 2. Inner view of the meshed burner model

Figure 3. vertical lines locations

and Presser [4], quite a few profiles at the exact location matching the experimental work and the surrounding region are obtained and diagrammatically shown in fig. 3, commonly referred here as vertical and horizontal lines (not shown here). The horizontal lines span the exit cylindrical diameter along the Z-direction at stream-wise location covering the range 0.416-0.486 m (with an increment of 1 cm) at the central Y-location ($Y = 1.1176$ m). In a similar fashion, would be the vertical profiles. Hence, the co-ordinate of the first horizontal line is (0.416, 1.1176, (–0.16, +0.16)). These profiles are used to validate the current computational work with the experimental data. Further results in terms of contours to the different parameters involved are also presented to give further insight on the spray combustion of liquid methanol (CH_3OH) using the models presented in this study.

In most of their readings, Widmann and Presser [4], estimated a percentage errors for most of the data obtained (for example the sonic nozzle used to spray liquid methanol has a manufacturer uncertainty of order 3%) and hence one would expect a difference in results between the CFD predictions for this case and the experimental data.

Table 2. Operating conditions for the baseline experiment of Widmann and Presser [4]

Fuel type	Fuel flow rate	Fuel temperature	Equivalence ratio	Air flow rate	Air temperature	Flame standoff distance	Chamber pressure
Methanol	3.0 kg/h	Ambient	0.3	56.7 m^3/h	Ambient	5	Ambient

Results analysis and validation of the CFD results

One adequate data-set offered by the experiment of Widmann and Presser [4] are the gas temperatures on thirteen points located at the exit pipe. Using the SDRM, the CFD results obtained from the simulation at the exact location as in the experiment of Widmann and Presser [4] is plotted in fig. 4. The figure clearly shows that the predicted results are in very good agreement with the experimental data. There is slight noticeable difference at the last two stations despite the agreement in trend between the CFD results and data at these two station. Such difference is expected as modelling such complex unsteady reactive flow using advanced reaction mechanisms. The agreement between the SDRM results and experimental data is also good when other parameters including carbon oxides and water vapour content are examined which

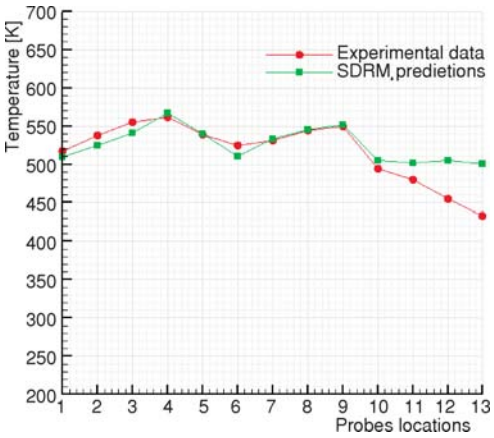

Figure 4. Comparison between the computational results for the methanol simulation using SDRM

will be presented later in the manuscript. Overall, the results shown in fig. 4 offer one good point, the validity of the set-up used in the computational model. It is clear that the way the problem was set in Fluent is correct and the predicted results are representatives and one can confidently rely on the model set-up to model the rest of the required benchmarks sought in the paper.

Temperature prediction using the EGRM

Following the SDRM simulation, the EXGAS was used to generate an advanced reaction mechanism for methanol (CH_3OH), methyl decanoate ($C_{11}H_{22}O_2$) (a biofuel), and n-decane ($C_{10}H_{22}$) (a conventional fuel). This mechanism is referred to here as EGRM as mentioned previously. The details of the whole reaction mechanism are too large to be covered in this manuscript. To give the reader a sense about the number of species and reactions involved, and in comparison to the SDRM used for methanol, the EXGAS mechanism for methanol contains species of order two folds to the SDRM and reactions about more than three folds the number of reactions for the SDRM. The larger the hydrocarbon such as n-decane, the larger the expected number of intermediate species and reactions.

Temperature profiles within the proximity of the exit of the burner (corresponding to the horizontal lines shown in fig. 3 were obtained from the three simulations that uses the EGRM. These horizontal lines are labelled by their X, Y, and Z-locations and/or range such as (0.416, 1.1176, (–0.15, 0.15)). This is shown in fig. 5 for methanol and in figs. 6 and 7 for n-decane and methyl decanoate, respectively.

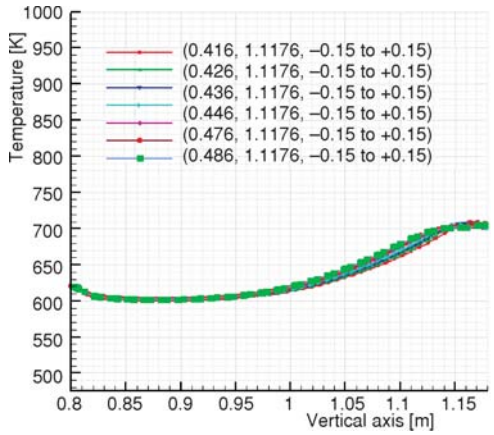

Figure 5. Temperature profiles corresponding to the horizontal lines shown in fig. 3 for the EGRM simulation for methanol

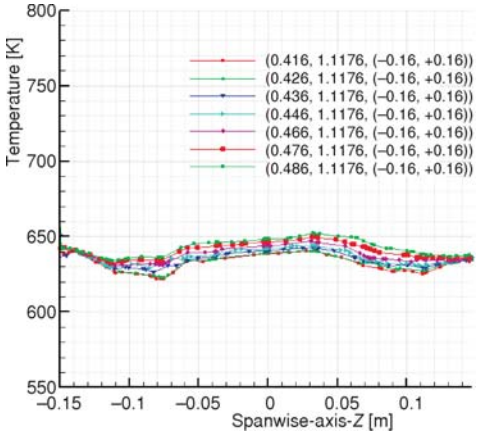

Figure 6. Temperature profiles corresponding to the horizontal lines shown in figure 3 for diesel CFD simulation using EGRM-diesel

For methanol, fig. 5, one can see that the temperature range predicted by the EGRM is higher than that predicted by the SDRM and the experimental data. The methanol EGRM temperature predicted range is 620-700 K which is higher than the experimental values (433-567 K). Two questions arise here: the first is why the simulation based on the EGRM model predicted higher temperature range than the experimental value, and the second is why the EGRM simulation predicted higher temperature than the SDRM simulation for the low-hydrocarbon, Methanol.

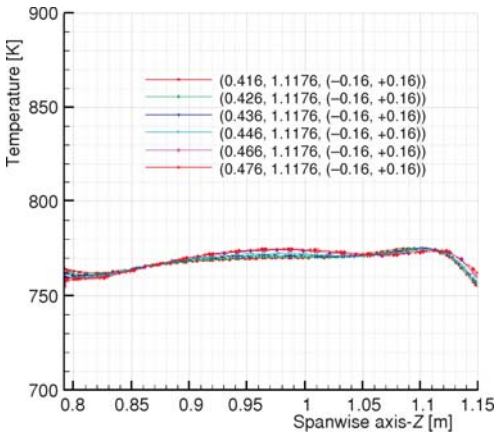

Figure 7. Temperature profiles corresponding to the horizontal lines shown in fig. 3 for biodiesel CFD simulation using EGRM

The best way to explain the points raised in the previous paragraph is to focus on the difference in species involved and the reaction steps considered when the EGRM model was developed. Examining the two mechanisms it is apparent that there is a large difference both in the number of species used as well as the number of reactions steps. Broadly speaking, one would state that the species used in SDRM are mainly the primary species considered by the EGRM. Neither secondary molecules (species) nor five types of radicals considered in the EGRM are included in the SDRM. The EGRM used in this work is considered an optimised one rather than the comprehensive one originally generated by the EXGAS software [10]. Some reaction rates and relevant kinetic data were carefully examined and compared with other available data like that of Burkast [14] to ensure accuracy of the data involved.

The radicals have been the subject of scrutiny. Their importance and whether to involve them in the EGRM has been a subject of a debate in the [15] with some experts in the field. It is apparent that any detailed reaction mechanism associated with the combustion of any hydrocarbon becomes more complicated as a result of the diversity of molecules and radicals involved. Not only that, the complexity is enhanced by the transient (time dependent) nature of the evolution of the combustion process with the chain mechanism (branching) of radicals playing crucial role making the process self-accelerated. The behaviour of the resultant intermediate products (elements) depends mainly on temperature leading to different evolution of the combustion process at different temperatures.

Other issues to be considered here is the fact that most of the studies cited in the literature are mainly seeking to model the kinetics of the combustion of such hydrocarbons in stable systems (shock tubes). Turbulence is well-known to enhance the mixing process and it is very relevant to non-premixed combustion systems such as the case of the current burner under consideration. When turbulence is taken into consideration, it will add another dimension to the complexity of the evolution of the combustion process and hence it is most unlikely that experimental and numerical simulation match each other.

Another aspect is the nature of the spray combustion used. All these reaction mechanisms were developed for the gas-phase oxidation and combustion of specific type of hydrocarbons. Therefore, if they are applied for the combustion of a hydrocarbon on a gaseous phase they may perform very well as the reaction steps come closer to the assumption made when these mechanisms were developed. As an example, the software used in this study (EXGAS) was vali-

dated for the gas-phase oxidation of quite a few fuels including several alkanes. This includes the study of Wrath *et al.* [16] who considered many alkanes including n-butane, n-heptane, iso-octane, n-octane, n-decane, and mixtures of n-heptane and iso-octane. The autoignition of iso-butane and iso-pentane in a shock tube from 1100 to 2000 K were studied by Oehlschaeger *et al.* [17]. However, there are many differences between the current case study and the studies mentioned. First, in the current work, spray combustion is involved where the initially liquid-phase fuel has been sprayed in the form of droplets with varying diameters. It would have been more informative if some information about the size of such droplets was available. However the versions of the software used do not provide this information. Although small in diameter, the combustion of such droplets is not instantaneous and takes a fraction of a second to burn leading to what is commonly known as delay period. The evaporation of such droplets takes place around the peripheries while leaving the fuel surrounding the centre to be in liquid phase. This process continues while the droplets travel randomly and interact with other droplets in many ways that affect the dynamics of combustion. While travelling in such turbulent flow, droplets eventually vaporise and burn completely although the word completely is not 100% correct as some of the by-products of any combustion is unburned hydrocarbon which sometimes includes element of the fluid itself in addition to other intermediate by-products. Therefore, the mechanism is not tested or used to model the combustion of liquid hydrocarbon in a form of a spray. The option of choosing higher temperature to generate the reaction mechanism while ignoring kinetics at lower temperature may also explain part of the difference. If lower temperature was chosen, the scenario might have been different. Having said so, most of the literature indicates that such reaction mechanisms are used to model the combustion process of some hydrocarbons at temperatures about 1000 K and, within these arrangements, limited attention was paid to reactions and species that are most likely to happen at lower temperature [18]. In spray combustion, the core of the droplet is much colder than the surrounding air and latent heat of vaporisation is absorbed from the surrounding hot gases to help in the vaporisation (gasification) process to enable burning of the liquid fuel. Hence, lower temperature reactions might be of importance to model spray combustion. However, the available literature indicates that it is not simple to design a reaction model that takes care of chemical kinetics at both high and low temperatures, mainly as a result of the very large number of possible reactions and intermediate products involved.

All this explains the fundamental difficulties in developing a reaction mechanism that accurately models both low-, medium-, and high-temperature expected regions in a domain where the combustion process is taking place. There is also uncertainties underlying the science of generating such comprehensive mechanism and using them in environments different than that for which they are mainly developed.

Temperature field for the EGRM of diesel and biodiesel

Consulting with fig. 6, the EGRM simulation of diesel produced an exit temperature of order 665 K. In comparison with the results obtained for methanol simulation using the SDRM (fig. 5) where the predicted values are in the range 505-515 K, it is apparent that the combustion of diesel led to a higher temperature range. Although there are no experimental data to reference here, one would say that these results are realistic with the percentage increase in temperature range for diesel is of order:

$$\frac{665-510}{510}=30\%$$

bearing in mind that diesel has slightly less than twice the calorific value of methanol.

The temperature profiles at the exit of the burner for methanol using EGRM predict slightly lower range than the case of diesel which still supports the validity of the diesel simulation using an EGRM.

The predicted temperature profiles using the EGRM for biodiesel at the exit of the burner are shown in fig. 7. As discussed in the beginning of this chapter, biodiesels are expected to yield lower value of energy (by the order of 10-15%) based on the measured calorific value which is documented in many studies and other related works. However, the temperature at the exit of the burner (fig. 7) shows a range of 740-760 K compared to 665 K for diesel simulation using EGRM, which is slightly higher.

It might seem like an obvious discrepancy in modelling biodiesel at this point. However, prediction of higher temperature using EGRM was observed in modelling methanol earlier, a fact that was stated by the developers of EXGAS even when only the kinetics of combustion were modelled with no turbulent flows having been taken into account. What is unique in this situation, however, is the fact that the same EXGAS used for biodiesel produced higher temperatures than diesel. There are two main issues the authors of this manuscript would raise in an attempt to explain the difference in the expected results for modelling biodiesel. Firstly, one may attribute this to the unsteady nature of the flow which cannot be captured very accurately by the steady simulation used in the current study.

The second fundamental issue to be raised here to explain the difference in temperature range observed for biodiesel simulation is the nature of the reaction model developed using the EXGAS software. Although the software includes the class of such biofuels, the EXGAS software seems to produce data for oxygenated fuels that needs further scrutiny. Developing an in-depth knowledge and analysis of the chemistry used in the EXGAS is beyond the scope of this manuscript, however, we strongly believes that any further work in this area should focus on studying the chemical reactions used in EXGAS and how the intermediate products are developed under a turbulent flow environment for conventional and oxygenated fuels. Examining the reaction model, it is clear that more reactive intermediate products were produced for biodiesel than diesel. could be due to the existence of the oxygen atoms and hence may have led to more reactions and heat liberation thus leading to higher temperature range that contradicts the fundamentals of combustion of conventional diesel compared to biodiesel.

To shed more light on the temperature field, spanwise cross-sectional profiles starting at close proximity of the injector at $Y = 0.2$ m from the base and increasing by 0.05 m increment along the vertical coordinate are taken from the four simulations. For the SDRM simulation, the corresponding temperature profiles are shown in fig. 10. The same profiles for the EGRM methanol simulation, diesel and biodiesel are, respectively shown in figs. 11, 12, and 13.

For the SDRM simulation for methanol, the temperature at close proximity to the injector ($Y = 0.2$ m) is quite high (of order 1200 K), decreasing gradually upon moving along the normal axis to a value of order 500 K, which is the average temperature of the whole burner, in agreement with the experimental work of Widmann and Presser [4]. This behaviour elucidates the structure and the length of the flame. Figure 10 clearly indicates that the flame length is of order 0.4 m and considering the length of the injector height from the base of the burner, the estimated flame length is of order 0.35 m. The figure also shows that the maximum width of the flame is of order 0.1 m.

For the EGRM simulation of methanol, The figure shows adequate symmetrical profiles along the centre with a maximum temperature (close to the injector location) of order 1600 K. Comparing this figure with its correspondence from the SDRM simulation (fig. 10), it is clear that

the EGRM model predicted slightly higher temperatures compared to the ones obtained using the SDRM but a better flame structure.

To support this point, temperature contours for a central x-y plane ($z = 0$) for both the methanol SDRM and EGRM simulations are shown in figs. 8 and 9, respectively. The contours provide a clear 2-D image of the flame structure and the distribution of temperature in the burner in general. For the SDRM simulation, the image displays a short, but a well-established flame.

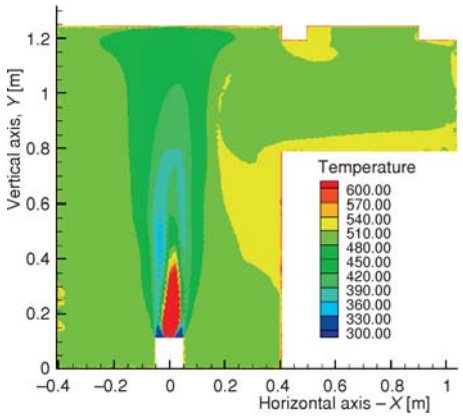

Figure 8. Methanol temperature contours for a central slice – SDRM simulation

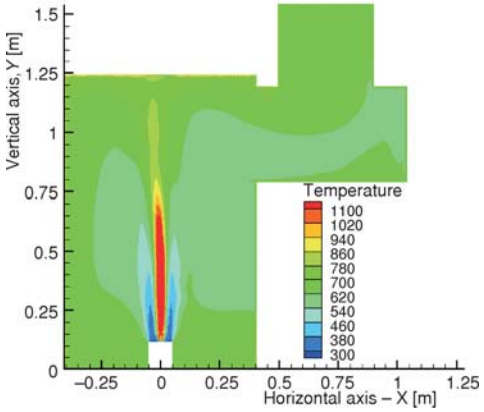

Figure 9. Methanol temperature contours for a central slice – EGRM simulation

It is more interesting when looking at fig. 9 which shows the temperature contours of the methanol EGRM simulation at a central slice similar to that shown in fig. 8. Both of figs. 9 and 11 indicate that the flame structure of the EGRM is much more realistic and displays similar features predicted by the SDRM but slightly longer and extends for a considerable distance along the vertical axis. This feature is is better seen from figs. 14 and 15 displaying the cross-sectional profile for the mixture fraction for the methanol simulation with the SDRM and EGRM, respectively. It is clear that at the same height, the burning species concentration is much higher for the EGRM than that for the SDRM which support the slow burning rate when

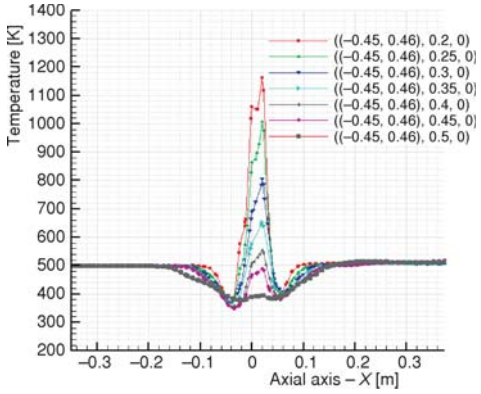

Figure 10. Cross-sectional temperature profiles close to the injector for methanol SDRM simulation

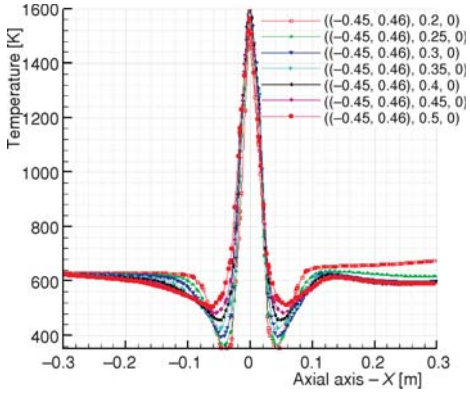

Figure 11. Cross-sectional temperature profiles close to the injector for methanol EGRM simulation

more species is involved. This fact holds the key to explaining the high temperatures especially at the measuring stations (fig. 5) observed for the case of the EGRM simulation. Whilst the SDRM simulation shows a flame that extends up to $Y = 0.4$ m, the EGRM prediction shows that the flame extends to a distance of order $Y = 0.7$ m along the normal axis. Having a hot region with temperature equivalent to the burning temperature of methanol up to almost half of the computational domain has contributed to the generally higher temperature range of the burner interior and at the exit.

For the diesel simulation cross-sectional temperature profiles (fig. 12) there are two distinct observations. The results show that the inner temperature for the diesel simulation is of order 650 K while that for the methanol is of order 500 K. The second observation is related to the maximum temperature attained in the case of diesel and methanol where at $Y = 0.2$ m, the methanol reports slightly higher temperature, 1190 K compared to 1000 K in the case of diesel. As discussed before, over-prediction of temperature seems to be a feature of the EGRM simulation. Also, while the low-carbon methanol is easy to predict with many advanced reaction mechanisms which have been developed and validated, large hydrocarbons such as diesel and biodiesel are still in progress.

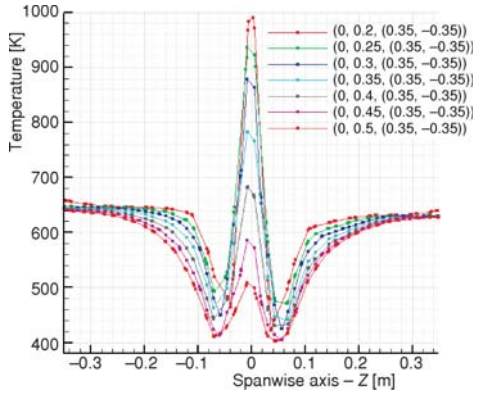

Figure 12. Temperature profiles corresponding to cross-sectional lines starting 0.2 m from the burner bottom for diesel CFD simulation using EGRM

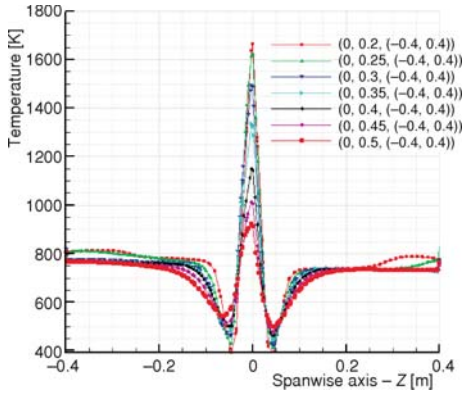

Figure 13. Temperature profiles corresponding to cross-sectional lines starting 0.2 m from the burner bottom for biodiesel CFD simulation using EGRM

For the biodiesel simulation, the lower temperature profiles (fig. 13) show a higher range close to the injector $T = 1605$ K compared to $T = 1000$ and 1119 K for methanol and diesel using EGRM. Probably this is the main reason why high temperature range was witnessed at the exit of the burner in the case of biodiesel. It is also noticeable that the average temperature for the rest of the interior domain of the burner is of order 800 K for the biodiesel simulation compared to 650 K for the modelling of diesel combustion (fig. 13). Worth to mention the experiment of Widmann and Presser [4] did not report data similar to the cross-sectional profiles presented.

Emission predictions

To shed more light on the validity of the CFD results and the developed reaction mechanisms, the predicted concentration (mole fraction) of CO_2 for the four simulations (SDRM for methanol and the EGRM for methanol, diesel and biodiesel) was compared with the experimen-

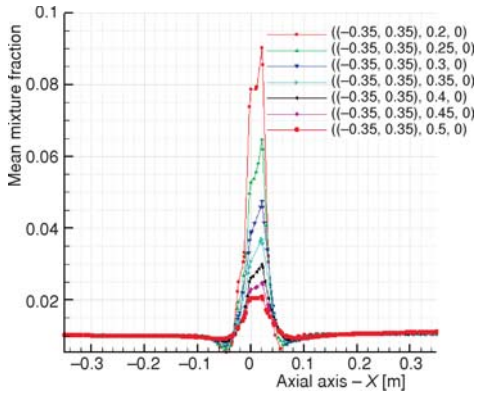

Figure 14. Mean mixture fraction profiles corresponding to cross-sectional lines starting 0.2 m from the burner bottom for methanol CFD simulation using SDRM

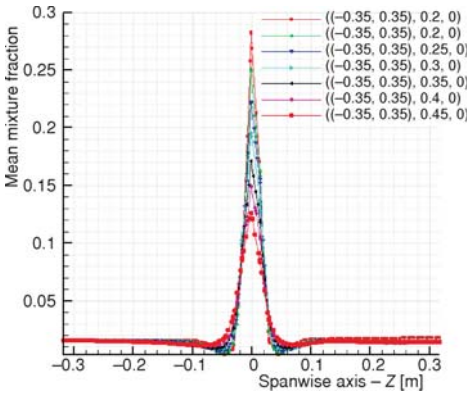

Figure 15. Mean mixture fraction profiles corresponding to cross-sectional lines starting 0.2 m from the burner bottom for methanol CFD simulation using EGRM

tal data in fig. 16. For the methanol SDRM simulation, the CFD results shows acceptable agreement with the experimental data, slightly under predicting the experimental values but by a small marginal difference. The difference could be due to many issues including the uncertainty surrounding the experimental data as old FTIR spectroscopy are used to determine the CO_2. We strongly believe that using advanced reaction mechanisms which include many intermediate species and reaction steps would definitely lead to a difference in results, but to the positive side rather than on the erroneous side. Based on these arguments, the predictions shown in this work so far are realistic and probably more accurate.

For the methanol simulation using the EGRM, the figure clearly shows that the prediction of CO_2 is very accurate as can be seen from fig. 16. This is a strong indication that the comprehensive reaction mechanism used is indeed necessary for predicting emission since the comprehensive mechanism predicted much closer values to the experimental data than that predicted by the reduced SDRM. For the diesel EGRM simulation, two observations can be made. The first is that the rates of the emission of CO_2 from diesel are higher in comparison with methanol. That is expected as heavier hydrocarbons can indeed produce higher carbon oxides due to the existence of large amount of carbon content in their structure, although the rates depends on other parameters including the boundary conditions of the combustion. The second is that the predicted rates of CO_2 exceed that of the experimental values at some measuring stations but lag a slightly below the experimental values at some other measuring stations. Nevertheless, the difference (positive or negative) is very small. Overall, one would say that EGRM-diesel has produced very good results for CO_2 and predicted this variable well.

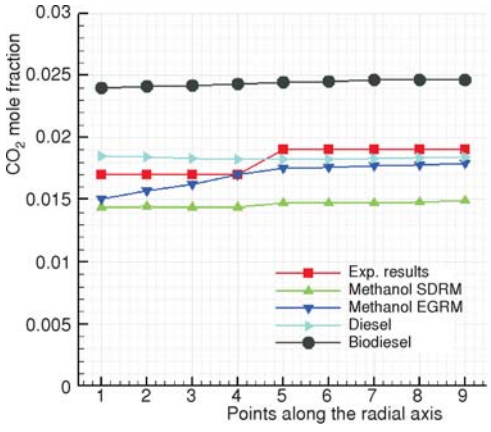

Figure 16. CO_2 comparison between the experimental, SDRM and EGRAM simulations for methanol, diesel, and biodiesel

For the biodiesel case, it is apparent that the EGRM model produced an elevated level for CO_2. For methanol (using EGRM), the predicted mole fraction for CO_2 values at the exit ranges between 0.0096-0.0149 with 0.07 near the injector (fig. 17). This is compared to 0.016-0.0185 at the exit locations for the diesel simulation (using EGRM) with 0.045 near the injector (fig. 18). For biodiesel, the mole faction of CO_2 at the exit locations ranges between 0.023-0.025 with a value slightly above 0.1 near the injector (fig. 19). It is apparent that the EGRM predicted slightly higher rates of CO_2 within the flame region for both methanol and biodiesel compared to diesel. However, these results agree with the findings of many other

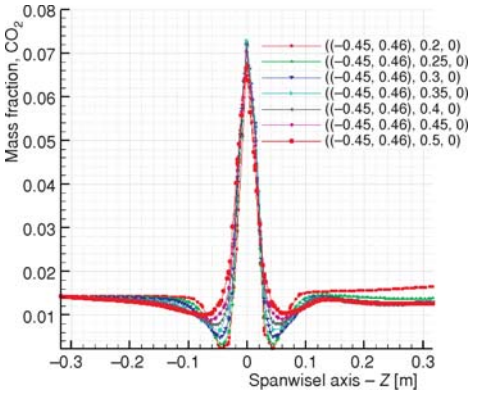

Figure 17. Cross-sectional profiles of CO_2 mole fraction close to the injector for methanol EGRM simulation

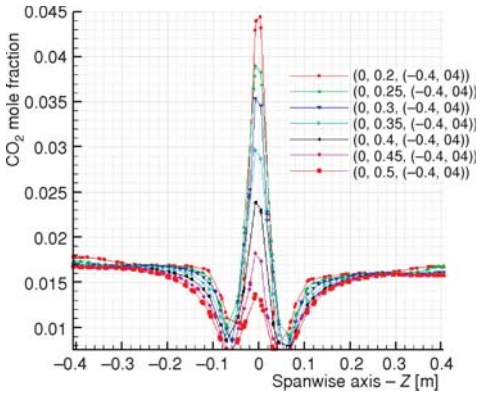

Figure 18. Cross-sectional profiles of CO_2 mole fraction close to the injector for diesel EGRM simulation

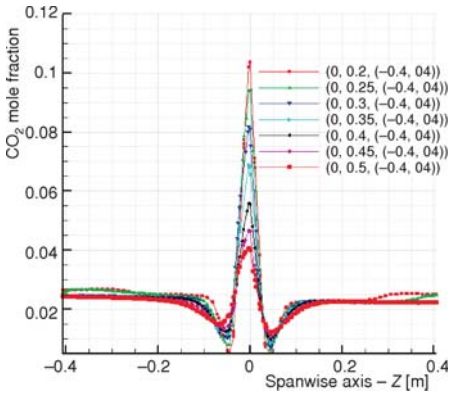

Figure 19. Cross-sectional profiles of CO_2 mole fraction close to the injector for biodiesel EGRM simulation

studies cited in [3] although the combustion infrastructure may differ from the current environment under consideration. Biodiesel indeed produces higher rates of both soot and CO_2, which is likely due to two factors. The first is associated with the oxygenated nature of biodiesel which influences the combustion process of biodiesel favouring the formation of CO_2. However, this property may also impact the way EXGAS generates the necessary reaction mechanism for such classes of fuels as mentioned earlier. The second reason is probably associated with the density and viscosity of biodiesel and this is mainly related to the experimental part. Overall, the prediction of EGRM for CO_2 in the simulation of biodiesel considered here is at acceptable levels and agrees with the literature.

Conclusions

The study used both reduced and comprehensive reaction mechanisms to model both light and heavy hydrocarbon from conventional and oxygenated fuels. The results show good agreement with the available experimental data, however, there are some differences that need

further consideration and investigation. Two generic findings from the results can be stated. The first was that the comprehensive mechanism which includes much more species and reaction steps has led to a delay in the combustion of the injected fuel leading to realistic flame structure but higher temperature when compared to the experimental values. The second was that the comprehensive mechanism has led to better prediction of emissions, a strong indication to the importance of including all possible intermediate species and associated reaction in accurately modeling reactive flows. More fundamental work is needed to understand the factors associated with developing advanced reaction mechanisms for oxygenated fuels in particular.

References

[1] Nigama, P. S., Singh, A. Production of Liquid BioFuels from Renewable Resources, *Progress in Energy and Combustion Science, 37* (2011), 1, pp. 52-68,
[2] Demirbas, A., Progress and Recent Trends in BioFuels, *Progress in Energy and Combustion Science, 33* (2007), 1, pp. 1-18
[3] Xue, J., *et al*., Effect of BioDiesel on Engine Performances and Emissions, *Renewable and Sustainable Energy Reviews, 15* (2011), 2, pp. 1098-1116
[4] Widman, J. F., Presser, C., A Benchmark Experimental Database for Multiphase Combustion Model Input and Validation, *Combustion and Flame, 129* (2002), 1, pp. 47-86
[5] Collazo, J., *et al*., Simulation and Experimental Validation of a Methanol Burner, *Fuel, 88* (2009), 2, pp. 326-334
[6] Poinsot, T., Veynante, D., *Theoretical and Numerical Combustion*, 2nd ed., RT Edwards, Philadelphia, Penn., Pasadena, Cal., USA Inc., 2005
[7] Menter, F. R., Two-Equation Eddy-Viscosity Turbulence Models for Engineering Applications, *AIAA Journal, 32* (1994), 8, pp. 1598-1605
[8] Peters, N., Laminar Diffusion Flamelet Models in Non-Premixed Turbulent Combustion, *Progress in Energy and Combustion Science, 10* (1984), 3, pp 319-339
[9] ***, ANSYS Inc., ANSYS Fluent 12.1 Theory Guide, 2009
[10] Warth, V., *et al.*, Computer Based Generation of Reaction Mechanisms for Gas-Phase Oxidation, *Computers and Chemistry, 24* (2000), 5, pp. 541-560
[11] Ranzi, E., *et al.*, A New Comprehensive Reaction Mechanism for Combustion of Hydrocarbon Fuels, *Combust. and Flame, 99* (1994), 2, pp. 201-211
[12] Herbinet, O., *et al*., Modelling Study of the Low-Temperature Oxidation of Large Methyl Esters from C11 to C19, *Proceedings,* Combustion Institute. Vol. 33, no. 1, pp. 391-398, 2011
[13] ***, http://garfield.chem.elte.hu/Burcat/burcat.html. [Accessed: August 1, 2012]
[14] ***, Chemical-Kinetic Mechanisms for Combustion Applications, San Diego Mechanism Web Page, Me- chanical and Aerospace Engineering (Combustion Research), University of California, San Diego, Cal., USA
[15] Wallington, T. J., *et al*., Automotive Fuels and Internal Combustion Engines: a Chemical Perspective, *Chemical Society Reviews, 35* (2005), 4, pp 335-347
[16] Warth, V., *et al*., Computer Aided Derivation of Gas-Phase Oxidation Mechanisms: Application to the Modelling of the Oxidation of n-Butane, *Combustion and Flame, 114* (1998), 1-2, pp. 81-102
[17] Oehlschaeger, M. A., *et al*.,Shock Tube Measurements of Branched Alkane Ignition Times and OH Concentration Time Histories, *International Journal of Chemical Kinetics, 36* (2004), 2, pp. 67-78
[18] Sarathy, S. M., *et al*., Comprehensive Chemical Kinetic Modelling of the Oxidation of 2-Methylalkanes from C7 to C20, *Combustion and Flame, 158* (2011), 12, pp. 2338-2357

Paper submitted: November 6, 2014
Paper revised: March 7, 2015
Paper accepted: March 19, 2015